Changes of Diurnal Temperature Range in Taiwan (1950-2007)

Shu-Ping Weng
Department of Geography, National Taiwan Normal University

Abstract

This study employed a trend EOF (TEOF) method to analyze the long-term (1950-2007) changes of diurnal temperature range (DTR) in Taiwan. Three statistically significant modes stand out. The TEOF1 depicts a monotonic decreasing trend of DTR, which is island wide except at Pengchiayu, Chengkung, Kaohsiung, and mountainous Yushan. The Mann-Kendall's tau (τ) rank correlations reveal that the increasing rate of daytime maximum (Tmax) at these stations is larger than the nighttime minimum (Tmin), thereby an increasing trend of DTR. The island wide reduction of DTR is closely related to the suppressed/enhanced cloud amount (CLD) during the daytime (nighttime) hours. The decreasing trend of Tmax in the western plains is consistent with the tendency in southeast China. The TEOF2 (TEOF3) depicts the low-frequency variations of DTR in central (northern) Taiwan. In both modes, the positive (negative) phase of DTR is attributed to the coordination between the positive (negative) phase of Tmax and negative (positive) phase of Tmin. Interestingly, the amplitude of TPC2 time series has an amplifying tendency after 1980. The connections between the regional DTR changes and global temperature extremes, and large-scale features in East Asia-tropical Pacific are also investigated. The results show that (1) the TEOF1 is related to global warming signal and likely regional anthopogenic emission as well; (2) the TEOF2 (TEOF3) is connected with the interdecadal changes of SST in the eastern (central) tropical Pacific Ocean.

Key word: DTR, global warming, trend analysis, ENSO, East Asian monsoons

1. Introduction

The diurnal temperature range (DTR), daytime maximum (T_{max}) minus nighttime minimum (T_{min}), measures the daily surface heat budget and is a popular climate index used to represent the local climate character. Due to the contrasts in heat capacity and moisture supply between the land and ocean, regions with a typical continental (oceanic) climate have a larger (smaller) mean DTR. Affected by the counteracting change between the surface shortwave and longwave radiation flux, the DTR also serves as the thermometer of our warming world since the late 19th century. As the global mean surface air temperatures (SAT) have risen by 0.74°C, the DTR also have decreased by 0.38°C over the last 50 years (IPCC 2007). This reduction in many places is observed as a result of temperatures increasing faster at night than during the day (Easterling et al. 1997; Vose et al. 2005). It then appears most of the observed warming of SAT is occurring at night.

However, a decreasing DTR is against the warming scenario played by the observed increase in the greenhouse gases. Both T_{max} and T_{min} due to the anthropogenic forcing should have increased with a similar magnitude, as predicted by climate models (e.g. Braganza et al., 2004). Previous studies that have sought to explain this dilemma have concluded that the cloud cover and soil moisture, not well resolved by current climate models, act as strong negative feedback processes to cause the observed DTR variations (e.g. Dai et al. 1999; Stone and Weaver 2003). Increasing cloud cover, especially the low cloud, may reduce the daytime T_{max} and suppress the longwave heat losses at night thereby increasing T_{min}, hence a decreasing DTR.

As the climate models are criticized with deficiencies failed in producing an increasing cloud cover, some studies based on satellite measurements reported a steady decline rather than the expected increase in Earth's albedo since the late 1980s (Pallé et al. 2004; Wild et al. 2005). It turns out that the cause of decreasing DTR is still not well understood, neither is its linkage to the greenhouse forcing. Meanwhile some other studies have revealed more complicated geographical difference in DTR. The regional DTR on a seasonal basis might experience various degrees of reduced magnitude caused by the intra-distributional changes in seasonal T_{max} and T_{min}. As an example, Caesar et al. (2006) reported that the decreased DTR due to the increased T_{min} can be exacerbated by a decreasing T_{max} over southern China and USA in warm seasons, concurred with previous findings (Zhai and Ren 1999; Frich et al. 2002).

Having a decreasing DTR is not a matter of "business as usual" either. In India (Kumar et al. 1994) and eastern Canada (Easterling et al. 1997) the DTR has increased due to a decrease in T_{min}. Primarily caused by the changing surface solar radiation, recent increasing DTR in western (eastern) Europe since the 1970s (1980s) is subsequent to the decrease since the 1950 (Makowski et al. 2008), suggesting the decadal-to-interdecadal

variations of DTR. Instead of solar dimming (Ohmura and Lang 1989), recent increase in DTR is in line with the solar brightening (Wild et al. 2005) as the increasing rate of global-scale T_{max} starts to catch up with the increased T_{min} (IPCC 2007), a revival of greenhouse warming theory (Wild et al. 2007).

With a quite limited latitudinal extent, Taiwan is anchored in the very geographical location affected by East Asian monsoons. Surface climate in this island is predominated by the interaction between the complex terrain and seasonal reversal of regular monsoon flows. Nevertheless, the annually mean SAT at 6 major stations has risen by 1.0-1.4°C in the last century (Hsu and Chen 2002), a magnitude much larger than the contemporary global averaged 0.3-0.6°C (IPCC 1996), and is even rising at a faster rate in recent 50 years. Noticeably, the warming rate is larger in summer than in winter, in contrast with the trends observed at higher latitudes. The weakening of East Asian summer monsoon and increases in the surface evaporation through which the increased water vapor that enhances the greenhouse effect has been suggested as a possible cause. The DTR has also been decreased due to a larger warming in T_{min} since the 1970s (Liu et al. 2002), which is associated with the island-wide decreasing trend of sunshine duration. The increases in regional-scale cloud cover and/or cloud albedo as an indirect result of anthropogenic emission of aerosols from the western plains of Taiwan have been suggested to be the major factors. As suggested by LIU02 and HC02, both local and large-scale factors that are inter-related may cause the variability, including the trend and low-frequency components, in the regional DTR. It is thus desirable to have a methodology capable of decomposing the observed anomalies into different trend modes. This study will use a multivariate trend analysis based on the empirical orthogonal function (TEOFA, Hannachi 2007) to analyze the DTR variability in Taiwan and examine its teleconnectivity as well.

2. Data sets

The 58-yr (1950-2007) historical data with daily DTR, T_{max}, T_{min}, and cloud cover (CLD) at twenty-one meteorological stations operated by the Central Weather Bureau (CWB) of Taiwan and archived in the DBAR (Data Bank for Atmospheric Research) of National Taiwan University (http://dbar.as.ntu.edu.tw) are used as the basis of this study. To examine the associated large-scale features, three contemporary global historical datasets taken from U.K. Meteorological Office Hadley Centre (http://hadobs.metoffice.com) are employed. (1) The newly released HadGHCND, detailed in Caesar et al. (2006), is a gridded land-only dataset created using quality-controlled station observations of near-surface T_{max} and T_{min} compiled by the U.S. NCDC's GHCN (Global Historical Climatology Network)-Daily database. Note that current version of this dataset still has large missing values in Africa, India, and South America. (2) The HadMAT1/MOHMAT43 (Rayner et al. 2003) is a gridded dataset of nighttime marine air temperature (NMAT). (3) The HadSLP2r, an updated version of HadSLP2 by combining the near real time product of NCEP/NCAR reanalysis, was created using marine observations of SLP from ICOADS (International Comprehensive Ocean-Atmosphere Data Set) and global land observations from 2,228 stations. HadSLP2 was found to have stronger subtropical anticyclones and features at high latitudes of NH compared to the earlier HadSLP1 (Allan and Ansell 2006).

3. Methodology of TEOF analysis

The steps of performing the TEOFA are briefly summarized as follow. Readers should refer to Hannachi's original article for the detailed mathematical background.

Let the data matrix $\mathbf{X}$, $\mathbf{X} = [x_{ij}]$, $i \in (1, n)$; $j \in (1, s)$, denote the anomalous field composed of s variables (number of stations) and n samples (no. of months). Unlike the convenient correlation (or covariance) based EOF analysis, which is characterized by a non-invariant transformation while measuring the linear associations between variables, TEOFA performs an invariant monotonic transformation on the data matrix $\mathbf{X}$ prior to the spatiotemporal decomposition (via SVD), which is achieved by recording the time positions of sorted series for each variable. That is, the anomalous time series in each of the column vectors $\boldsymbol{x}_1, \boldsymbol{x}_2, \ldots, \boldsymbol{x}_s$, where

$$\boldsymbol{x}_k = (x_{1k}, x_{2k}, \cdots, x_{nk})^{\mathrm{T}}, k \in (1, s), \quad (1)$$

are sorted and the associated time positions (i.e., $1, 2, \ldots, n$) are used to form a new transformed matrix $\mathbf{Q}$ such that its elements in each column vector $\boldsymbol{q}_1, \boldsymbol{q}_2, \ldots$, and $\boldsymbol{q}_s$, where

$$\boldsymbol{q}_k = (q_{1k}, q_{2k}, \cdots, q_{nk})^{\mathrm{T}} = (Q_k(1), Q_k(2), \cdots, Q_k(n))^{\mathrm{T}}. \quad (2)$$

would satisfy the following inequality:

$$x_{Q_k(1),k} \le x_{Q_k(2),k} \le \cdots \le x_{Q_k(n),k}, k \in (1, s). \quad (3)$$

A close relationship between the time-sorted sequence $\boldsymbol{q}_k$ and the ranks of original data stored in $\boldsymbol{p}_k$:

$$\boldsymbol{p}_k = (p_{1k}, p_{2k}, \cdots, p_{nk})^{\mathrm{T}} = (P_k(1), P_k(2), \cdots, P_k(n))^{\mathrm{T}}, \quad (4)$$

has been proved in Hannachi (2007), which is rewritten in a more concise form as follows.

$$Q_k^{q_k(m)} = P_k(m), \text{and} \quad (5.1)$$

$$P_k^{p_k(m)} = Q_k(m), \; m \in (1, n). \quad (5.2)$$

Equation (5.1) says that, for the station k, we can know the rank of its *mth* observation $P_k(m)$ by cyclically shifting the *mth* position of Q_k sequence r times, where the integer r is the positioned value $q_k(m)$ at the same position. Inversely, based on Equation (5.2) we can also shift the *mth* position in the P_k sequence r' times, where

the integer r' is the ranked value $\boldsymbol{p}_{\kappa}(m)$, to recover the time position in the *mth* Q_k sequence. As a result, the time-sorted matrix **Q** is in fact an inverse-rank matrix of original data matrix **X**. Analyzing the spectrum embedded in matrix **Q** through the use of EOF technique provides a methodology for multivariate rank correlation analysis used for the multiple trend detection, if exists.

By means of the monotonicity in time series of each variable, it can be recognized that Equation (2) conditioned by (3) essentially denotes a nonlinear transformation between the original data matrix **X** and the new time-sorted matrix **Q**. Maximizing the common monotonicity between the variables (i.e., columns) gives the time positions where the variables, some or all, are increasing (or decreasing) together. The measure of the largest common monotonicity is achieved by seeking the largest variance of a linear combination of position sequences $\boldsymbol{q}_k$ via the convenient EOF technique. Firstly, a (s by s) symmetric covariance matrix **C** is formed from the matrix **Q** after being centralized by an operator **H**:

$$\mathbf{C} = \frac{1}{n}(\mathbf{HQ})^{\mathrm{T}}(\mathbf{HQ}), \text{where} \tag{6}$$

$$\mathbf{H} = \left(\mathbf{I}_n - \frac{1}{n}\mathbf{1}_n\mathbf{1}_n^{\mathrm{T}}\right). \tag{7}$$

The $\mathbf{I}_n$ is an identity matrix with dimensions n by n, and $\mathbf{1}_n$ is a column vector with n elements equaling to ones: $(1, 1, \ldots, 1)^{\mathrm{T}}$. Matrix **C** is then subjected to the SVD: $\mathbf{C} = \mathbf{V}\Lambda\mathbf{V}^{\mathrm{T}}$, to obtain the ordered (usually descending) eigenvalues λ_κ [$\kappa \in (1, s)$] stored in the diagonal of matrix Λ and associated eigenvectors $\mathbf{v}_\kappa$ stored in the columns of matrix **V**. Note that the left and right singular vectors are identical for a symmetric matrix **C**. The first eigenvector (κ=1) will maximize the common monotonicity (i.e., trend) quantified by the ratio of $\lambda_{\kappa=1}$ to $\sum_{\kappa=1}^{s}\lambda_\kappa$, and the second one ($\kappa$=2) will also maximize the same trend but is uncorrelated with the first eigenmode, and so forth for higher order modes. As a result, this method can also detect the local trends, if they can survive from statistical significance test. In this study, this is performed based on North's rule of thumb. The corresponding principal components (PCs) $\boldsymbol{\mu}_\kappa$ [$\kappa \in (1, s)$] stored in the columns of matrix **U** (with dimensions n x κ) can be obtained by projecting the centralized matrix **HQ** onto the eigenvectors $\mathbf{v}_\kappa$ stored in the columns of matrix **V**:

$$\mathbf{U} = \mathbf{HQV} \tag{8}$$

Note that both vectors $\boldsymbol{\mu}_\kappa$ and $\mathbf{v}_\kappa$ are located in the position-related state space rather than in the original anomaly-related state space. To return to the physical space, data matrix X is first projected onto the eigenvectors $\mathbf{v}_\kappa$ and then centralized by the operator **H** to yield the PC time series of trend modes $\tilde{\boldsymbol{\mu}}_\kappa$ stored in the columns of matrix $\tilde{\mathbf{U}}$:

$$\tilde{\mathbf{U}} = \mathbf{HXV} \tag{9}$$

Vectors $\tilde{\boldsymbol{\mu}}_\kappa$ are then scaled and regressed with the anomalous matrix **X** to yield the regression coefficients $\tilde{\boldsymbol{v}}_\kappa$ at each station. It is in Figures 1 and 2 that the PC time series $\tilde{\boldsymbol{\mu}}_\kappa$ and trend patterns $\tilde{\boldsymbol{v}}_\kappa$ ($\kappa = 1, 2, 3$) are shown, respectively.

4. Results of TEOF analysis

Although usually monotonic, a "trend" in this study means a general direction where a system tends to move systematically. Figure 1 shows the first three trend PCs of monthly-mean DTR'. The variance associated with the monotonic trend is fully explained by the TPC1 which occupied 17.2% of the total variance (Fig. 1a). The regression line also shows the change point of the sign-reversed occurs in the beginning of 1977, coherent with the well-known timing of Pacific climate regime shift. The next two modes (Figs. 1b and 1c) individually occupy a smaller fraction of the total variances (7.9% and 7.6%). Two intriguing features are noticed. *Firstly*, the amplitude of TPC2 is relatively larger (smaller) after (before) the 1976/77 regime shift. *Secondly*, the temporal evolution of TPC3 tends to be out-of-phase (in-phase) with that of TPC2 after (before) 1977. It is worthwhile to mention that the contribution of TPC2 and TPC3 together, 15.5%, is comparable with the 17.2% in TPC1. These two modes reflect the projections of the continental-scale variations onto the regional temperature changes and owe solid physical meanings

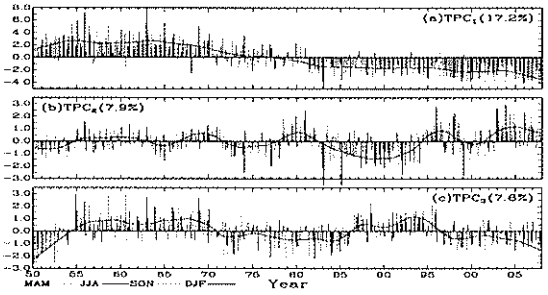

Fig. 1 The first three TPCs of time series in the monthly-mean DTR anomalies. Explained fractions (in percentage) of the total variance are given inside the parentheses. Superimposed are the locally weighted regressions using F=0.5 (thick dark lines). The monthly-mean amplitudes, which are drawn in different colors according to the standard seasons, are rescaled by the 1.0 s.t.d. of the *globally* monthly-mean DTR climatology.

The corresponding trend patterns (TEOFs) are shown in Figure 2a-c. The shown values, scaled by the radius of red/blue solid circles (in right-bottom corner), are the positive/negative regression correlations obtained by projecting the original monthly-mean DTR' across stations onto the individual TPCs. Stations with a larger value indicate the increased representative of the TPC time series for their time evolutions. The TEOF_1 (Fig. 1a) depicts an island-wide DTR' trend (red circles) while taking the decreasing TPC_1 into account (c.f., Fig. 1a). More importantly, the TEOF_1 also captures the DTR'

trend at four stations: PCY, CK, KH, and mountainous YS (blue circles). Among them, the CK station has the largest negative correlation.

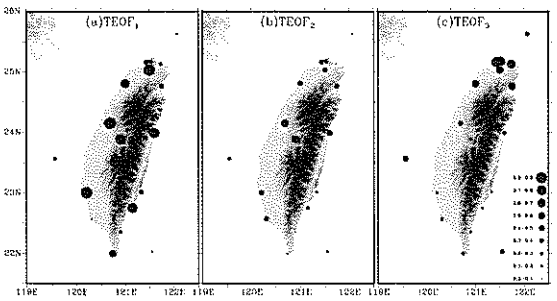

Fig. 2 The first three TEOFs obtained by regressing the TPCs (shown in Figs. 1) onto the original monthly-mean DTR anomalies at each station. The positive (negative) regression coefficients are colored in red (blue).

In contrast, spatial patterns in both TEOF2 (Fig. 1b) and TEOF3 (Fig. 1c) tend to be localized. Stations with larger correlations are located in the central and northern part of Taiwan, respectively. Combined with the slowly varying TPC2 (c.f., Fig. 1b), trend pattern in TEOF2 indicates that the associated DTR′ amplitude is relatively small before the 76/77 regime shift but amplifies thereafter over the central Taiwan, decreased in late 1980s and early 1990s but has increased since 1995. As for the TEOF3, although the trend pattern is clearly biased toward the northern stations, significant negative correlations, thereby oscillating in an opposite direction, also appear at TN and KH stations located in the southwestern corner (blue solid circles). As a whole, the in-phase (out-of-phase) relation between the TPC1 and TPC2 (TPC3) in late 1980s and early 1990s suggests an island-wide DTR^- trend during that period. Conversely, the in-phase (out-of-phase) relation between the TPC1 and TPC3 (TPC2) in recent decade indicates that the magnitude of DTR^- trend is still increasing in the northern Taiwan but slowing down in the central and southwestern regions.

The Kendall's τ values between the TPC1 and raw monthly-mean T'_{min}, T'_{max}, and CLD′ (available data in the 1961-to-2007 period) during the nighttime (CLD'_n; 18L-to-06L averaged) and daytime (CLD'_d; 07L-to-17L averaged) time series across stations is shown in panels of Figure 3. Stations with a positive/negative τ (marked as red/blue circles) represent an in-phase/out-of-phase relationship with the decreasing TPC1 time series, thereby having a decreasing/increasing trend (denoted as $(\bullet)^+/(\bullet)^-$). The dominant DTR^- trend is linked to an island-wide T^+_{min} (blue circles in Fig. 3a). Meanwhile, a predominant T^+_{max} trend (blue circles in Fig. 3b) is also seen in most stations. Interestingly, stations located in the west plains show a common T^-_{max} trend (red circles in Fig. 3b). The island-wide T^+_{min} trend thermally is consistent with the increase in nighttime cloud cover (i.e. CLD^+_n; blue circles in Fig. 3c). The prevailing T^+_{max} is also consistent with the overall CLD^-_d trend (red circles in Fig. 3d). Nevertheless, exceptions occur at TP and HC in the northern plain and PH in the Taiwan Strait where an opposite CLD^+_d is found (blue circles in Fig. 3d). Note that while such a trend at HC and TP is consistent with their T^-_{max} trend connected through the reduction of daytime solar irradiance and/or the enhanced planetary albedo, the CLD^+_d (CLD^-_d) at PH (TC, JYT, and ALS) cannot explain the associated T^+_{max} (T^-_{max}). In this respect, station at TC, the most populated city in the central Taiwan, is peculiar in that its T^+_{min} trend also contradicts the significant CLD^-_n trend (red circle in Fig. 3c). The same feature is also found at KH, another metropolitan city in the southern Taiwan. Inconsistencies between the changes in temperature extremes and cloud cover strongly suggest the existence of other low-frequency modes interfering with the monotonic trend and/or the human influence such as sulphate/aerosol emission and urbanization with their unnegligible contributions mistaken as the long-term trend by the conventional univariate analysis.

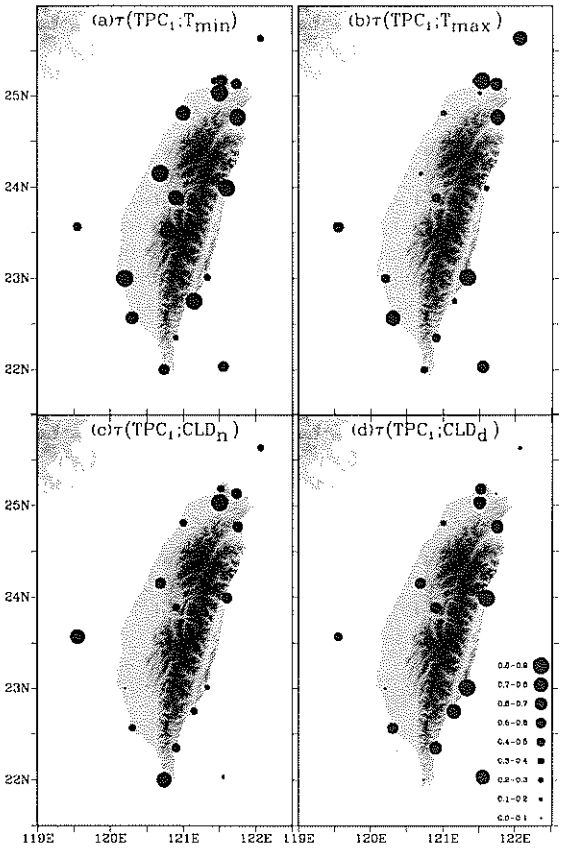

Fig. 3 Shown are the Kendall's τ between the TPC1 and monthly-mean (a) T_{min}, (b) T_{max}, (c) nighttime (CLD_n; 18L-06L), and (d) daytime (CLD_d; 07L-17L) anomalies. The positive (negative) τ values, the anomalous time series evolves in- (out-of-) phase with TPC1, are marked as red (blue) circles. The circle is filled (open) if (in-) significant at 0.05 level.

The T_{max}, T_{min}, day-to-night CLD anomalies associated with the TPC2 t.s., which is largely explained by the stations over the central Taiwan, are also examined. The phase of DTR^+, for example in recent

decade, is mainly attributed to the coherent T^{+}_{max} plus the aids from an anti-correlated T^{-}_{min} at the mountainous JYT, ALS, and YS stations (not shown). As a result, this low-frequency mode will counteract the TPC1-DTR^{-} trend by increasing the T_{max} at some stations such as TC and HL. In contrast, it will exacerbate the monotonic DTR^{+} trend at YS station by increasing the T_{max} while decreasing the T_{min}. In the TEOF2, as the correspondence between T^{+}_{max} and CLD^{-}_{d} can be connected through the enhanced daytime solar irradiance at most stations, the coherent relation between T^{-}_{min} and CLD^{-}_{n} via the enhanced nighttime heat losses is only valid at the mountainous JYT, ALS, and YS (not shown). Again, stations that have a T^{+}_{min} thermally inconsistent with the associated CLD^{-}_{n} signal are mainly located in the densely populated cities over the western plains. It implies that other climatic and/or non-climatic factors should come into play. Similar indications are also found in the distributions of τ values of T_{min}, T_{max}, CLD_n, and CLD_d anomalies that associate with the TPC3 which is largely explained by stations located in the northern Taiwan (not shown).

5. Large-scale associations

The Kendall's τ between the seasonally stripped time series of TPCs and global gridded anomalies in DTR, T_{max}, T_{min}, NMAT, and SLP are also examined to explore how the large-scale variability of surface thermal and circulation conditions in the Asian-Pacific monsoon regions and ENSO activity may cause the DTR change in Taiwan. Panels in Figure 4 show the spatial distributions of τ values for various quantities associated with the TPC1 in 4 seasons. Note that a reversed color/contour code is used to facilitate our discussions; the τ values of thermal quantities (i.e., DTR, T_{max}, T_{min}, and NMAT) and of SLP anomalies that are correlated (anti-correlated) with the decreasing TPC1 thereby having a decreasing (an increasing) trend are shaded by cool- (warm-) colors and contoured by dashed (solid) lines, respectively. Only when the τ values of thermal quantities (SLP) significant at 0.05-level (≥ 0.20 or ≤ -0.20) are the corresponding gridded points shaded (contoured at 0.1 intervals). A widespread DTR^{-} trend dominates the global landmass particularly in Eurasia. As this is due to the combination between the prevailing T^{-}_{min} and T^{+}_{max} at higher latitudes (north of 45°N) in DJF-MAM, over the central Asia in JJA-SON, and southwestern China-Indochina peninsula throughout the year, such a reduction in southeastern China and eastern USA is caused by the combination between the quasi-persistent T^{-}_{max} and season-dependent T^{+}_{mina}. The prevailing T^{-}_{max} (T^{+}_{min}) trend in the later (former) is associated with an in-situ SLP^{+} (SLP^{-}) trend. Nevertheless, while the persistent SLP^{+} trend over China seems to be a regional pattern in East Asia, the continental SLP^{-} in Siberia extends downstream into the north Pacific storm track region where an out-of-phase $NMAT^{-}$ trend (vs. T^{+}_{min} over landmass), most pronounced in MAM, exists. It features the cool ocean-warm land paradigm (COWL; Wallace et al. 1995) in a GHG warming world. Toward the deep Tropics, the T^{+}_{min} again dominates the T^{+}_{max} causing a DTR^{-} trend in

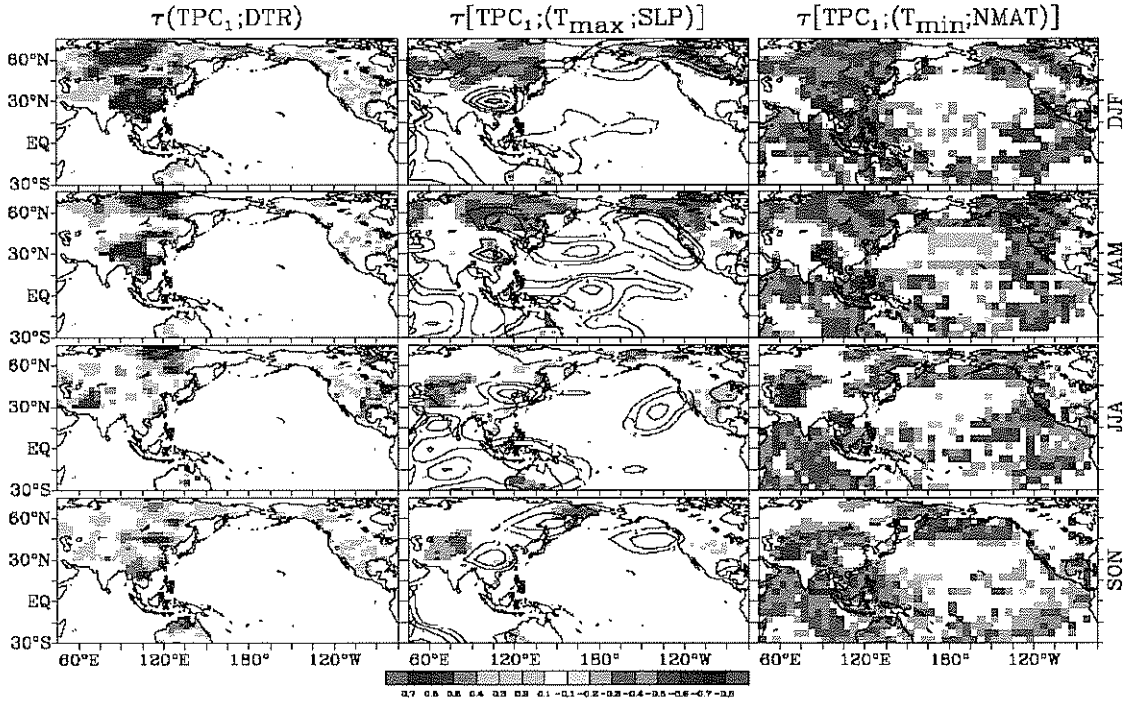

Fig. 4 The distributions of τ values between the seasonally-stripped monthly-mean TPC1 time series and HadGHCND DTR' (left panels), T'_{max} (middle panels), and T'_{min} (right panels) over the global landmass. The correlated SLP' (NMAT') archived in the HadSLP2r (HadMAT1) dataset is also contoured (color shaded) on the middle (right) panels with 0.1 intervals starting from ±0.05.

Mindanao, Borneo, and northern Australia. The warming land is found mainly associated with a year-round $NMAT^{+}$ trend over the surrounding waters and Indian Ocean-to-western Pacific, though it also has the indication of $NMAT^{-}$ signal in the tropical central Pacific where a significant SLP^{+} pattern evidences in MAM. Seasonally, the DTR^{-} trend and $NMAT^{+}$ in the surrounding oceans are most pronounced in SON. In contrast, only in few coastal regions of Malaya and Sumatra can the dominant T^{+}_{max} and hence a DTR^{+} trend appears in JJA. These large-scale seasonal features have their local correspondences in Taiwan

The distributions of τ values for various thermal quantities that correlate with the TPC2 in DJF (JJA) are shown in the left (middle) panels of Figure 5. The local DTR^{+} in DJF is associated with a continental-scale DTR^{+} pattern in Asian continent most significant in southeastern China (Fig. 5a), mainly attributed to the T^{-}_{min} rather than the T^{+}_{max} (Fig. 5c vs. 5b). The SLP^{+} pattern suggests a stronger winter monsoon in East Asia. As the cold dry air is advected over waters, increased upward heat fluxes may cause the $NMAT^{-}$ signal over the northwestern Pacific and South China Sea (Fig. 5c) thereby suggesting a stronger EAWM. The local DTR^{+} phase, which oscillates in a decadal-to-interdecadal timescale, also shows a strong teleconnection with the low-frequency variability in the tropical Pacific as well as tropical Indian Ocean. In particular, the $NMAT^{-}$ ($NMAT^{+}$) pattern in the eastern (western) Pacific cold tongue (warm pool) is associated with an intensified Pacific Walker cell that has a SLP^{+} (SLP^{-}) change to the east (west) of Date Line, a scenario reminiscent of La Niña condition. The above theme, a stronger EAWM is linked to La Niña condition in the tropical Indo-Pacific Ocean, persists into MAM (not shown).

In JJA although the local DTR^{+} that concentrates in the central mountainous region of Taiwan also has a partner over the highlands of Luzon, it is mainly associated with an out-of-phase DTR^{-} in Maritime Continent (Fig. 5d) attributed to the predominant T^{+}_{min} (Fig. 5f vs. 5e). This is in accordance with the $NMAT^{+}$ and SLP^{-} over the tropical western Pacific, suggesting the response of the lower troposphere to the warmer tropical oceans. Noticeably, the SLP′ pattern anchored in the waters around Indonesian-North Australian regions forms an arching wave train stretching from the western Pacific across the Aleutians to North America (Fig. 5d), reminiscent of Pacific-Japan pattern (Nitta 1987). In its passage, the SLP^{+} change around the normal monsoon trough region denotes the southwestward shift of Pacific subtropical high hence a weaker southwesterly monsoon.

Change of the large-scale circulation pattern in East Asian winter that associates with the TEOF3 depicts a weakened EAWM as revealed by the SLP^{-} change (Fig. 5g). In tropics, a weakened Walker cell signified by the SLP^{+} (SLP^{-}) change in Maritime Continent (eastern Pacific) together with the NMAT′ resembles a developing El Niño in the central tropical Pacific. The above scene that connects a weaker EAWM to an El Niño-like event is found relatively persistent in the preceding SON and subsequent MAM (not shown).

References

Hannachi, A., 2007: Pattern hunting in climate: a new method for finding trends in gridded climate data. *Int. J. Climatol.*, **27**, 1-15.

Hsu, H.-H., and C.-T. Chen, 2002: Observed and projected climate change in Taiwan. *Meteorol. Atmos. Phys.*, **79**, 87-104.

IPCC (2007) Climate change 2007: the physical science basis. Cambridge University Press, Cambridge.

Liu, S. C., C.-H. Wang, C.-J. Shiu, H.-W. Chang, C.-K. Hsiao and S.-H. Liaw, 2002: Reduction in sunshine duration over Taiwan: Causes and implications. *TAO*, **13**, 523-546.

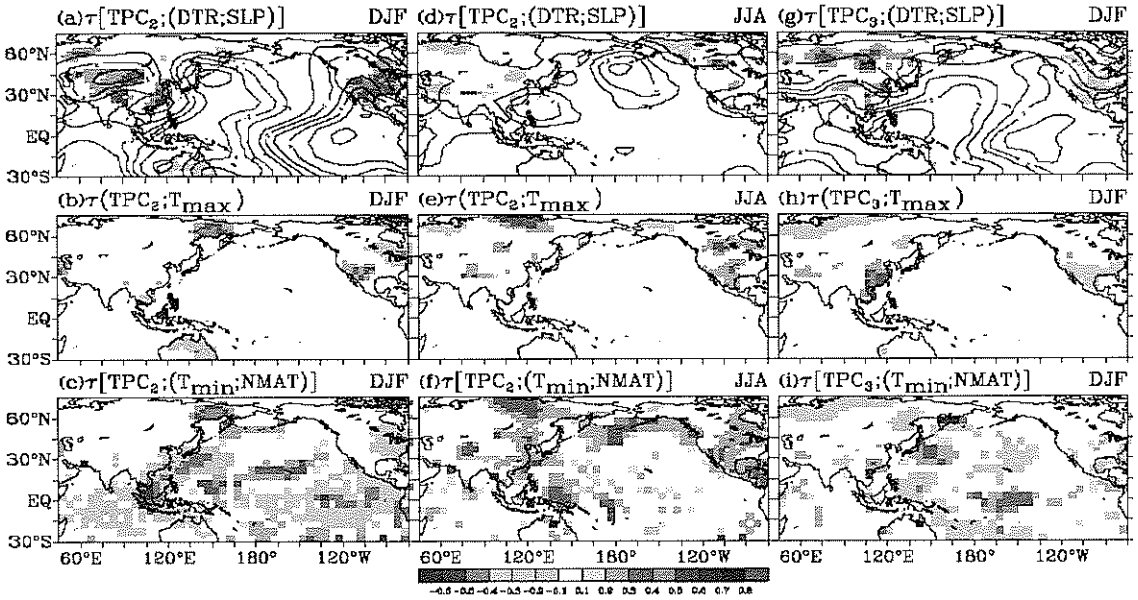

Fig. 5 Same as Fig. 4, but for the TPC2 and TPC3 related tau values in DJF and JJA seasons only.